Full characterization and analysis of a terahertz heterodyne receiver based on a NbN hot electron bolometer

M. Hajenius[a)]
Kavli Institute of NanoScience, Faculty of Applied Science, Delft University of Technology, Lorentzweg 1, 2628 CJ Delft, The Netherlands and SRON Netherlands Institute for Space Research, Sorbonnelaan 2, 3854 CA Utrecht, The Netherlands

J. J. A. Baselmans
SRON Netherlands Institute for Space Research, Sorbonnelaan 2, 3854 CA Utrecht, The Netherlands

A. Baryshev
SRON Netherlands Institute for Space Research, Sorbonnelaan 2, 3854 CA Utrecht, The Netherlands and Kapteyn Astronomical Institute, University of Groningen, 9700 AV Groningen, The Netherlands

J. R. Gao
Kavli Institute of NanoScience, Faculty of Applied Science, Delft University of Technology, Lorentzweg 1, 2628 CJ Delft, The Netherlands and SRON Netherlands Institute for Space Research, Sorbonnelaan 2, 3854 CA Utrecht, The Netherlands

T. M. Klapwijk
Kavli Institute of NanoScience, Faculty of Applied Science, Delft University of Technology, Lorentzweg 1, 2628 CJ Delft, The Netherlands

J. W. Kooi
California Institute of Technology, MS 320-47 Pasadena, California 91125

W. Jellema and Z. Q. Yang
SRON Netherlands Institute for Space Research, Sorbonnelaan 2, 3854 CA Utrecht, The Netherlands

(Received 24 November 2005; accepted 8 July 2006; published online 11 October 2006)

We present a complete experimental characterization of a quasioptical twin-slot antenna coupled small area ($1.0\times0.15\ \mu m^2$) NbN hot electron bolometer (HEB) mixer compatible with currently available solid state tunable local oscillator (LO) sources. The required LO power absorbed in the HEB is analyzed in detail and equals only 25 nW. Due to the small HEB volume and wide antenna bandwidth, an unwanted direct detection effect is observed which decreases the apparent sensitivity. Correcting for this effect results in a receiver noise temperature of 700 K at 1.46 THz. The intermediate frequency (IF) gain bandwidth is 2.3 GHz and the IF noise bandwidth is 4 GHz. The single channel receiver stability is limited to 0.2–0.3 s in a 50 MHz bandwidth. © *2006 American Institute of Physics*. [DOI: 10.1063/1.2354421]

I. INTRODUCTION

The spectrum between 1 and 6 THz contains unique spectroscopic lines of ions, atoms, and molecules that play a key role in understanding fundamental astrophysical and atmospheric processes. However, high resolution spectroscopic observations[1,2] in this frequency range are still extremely rare. This is because heterodyne spectrometers are not a well established technology at frequencies above 1 THz and radiation at these frequencies is strongly absorbed in the earth's atmosphere.

The increased accessibility of space has stimulated the development of heterodyne receivers[3] for this frequency range. Three crucial components have seen major improvements. Firstly, the development of tunable solid state local oscillator (LO) sources,[4] possibly in the future replaced by terahertz quantum cascade lasers.[5,6] Secondly, improved intermediate frequency (IF) amplifiers,[7] which benefit from major progress in telecommunication technology. Finally, the development of suitable mixing elements using superconducting hot electron bolometers (HEBs), which will be the focus of this paper.

NbN HEB mixers are the most sensitive detectors for spectrometers above ~1 THz. This makes NbN HEBs highly attractive for both ground-based[8] and space-based[9] telescopes for astronomy. Since the introduction of HEBs by Gershenzon *et al.*[10] and Prober,[11] considerable progress in both performance[12–16] and device physics[17–20] has been achieved.

The basic operating principle of HEBs utilizes the fact that terahertz radiation heats the electrons in the superconducting bridge. This induces a local resistance due to the dependence of the resistive transition intrinsic to the NbN film[19] (i.e., not of the full device structure) on the temperature and bias current.[20] To operate the detector adequately, a certain amount of LO power together with a dc bias voltage is required to bring the device to its optimal operating condition (Sec. IV C). The unknown terahertz radiofrequency (RF) signal is then mixed in the HEB with a LO signal and down-converted to an IF signal. The IF signal contains the

[a)]Electronic mail: m.hajenius@tnw.tudelft.nl

full information of the RF signal within the IF bandwidth (Sec. IV D), typically limited to several gigahertz, around the LO frequency.

Measurements on large area NbN HEBs contacted to highly conductive normal metal spiral antennas have demonstrated excellent sensitivities in the frequency range of 1–5.3 THz.[12,14–16]

Many practical applications require polarization sensitivity, making either waveguide mixers or quasioptical twin-slot antennas preferable. The advantage of twin-slot coupled HEBs is that they can potentially be operated at much higher frequencies, while they are still easy to realize using microfabrication techniques. We therefore focus on twin-slot antenna coupled NbN HEBs operated with a tunable solid state LO source.[4] An important issue is the limited LO power from currently available tunable LO sources[4] that can be coupled to the HEB. The latter is especially critical using our optical design discussed in Sec. III. Furthermore, for higher frequencies, the available solid state LO output power falls off rapidly due to reduced multiplication efficiency. The key to efficiently operate the HEB under these conditions is the reduction of the HEB's LO power requirement by decreasing its size to an area of $\sim 1.0 \times 0.15\ \mu m^2$. Although more efficient optical coupling schemes exist and terahertz LO sources with higher output power might become available, low LO power requirement is still attractive and even crucial for the application of HEBs in arrays.

The anticipated application of HEBs and the multitude of specialized reports on such mixers make the need for a complete and systematic description of all mixer parameters apparent. In this paper we present the full characterization of all relevant parameters related to the mixer performance by focusing essentially on one and the same twin-slot coupled small area HEB mixer. Such a systematic study is desirable from both an application and a device physics point of view. To understand which mixer properties are relevant we discuss how heterodyne terahertz spectroscopy using a small area NbN HEB is performed in practice.

The sensitivity of the receiver (Sec. IV A), usually expressed as an equivalent noise temperature at the input of the receiver (T_N), is determined by a standard laboratory calibration procedure. This method can be complicated by an unwanted direct response (Sec. IV B) that occurs in addition to the heterodyne response. This results in a calibration error if uncorrected. Hence, a direct response correction may be necessary, mostly for devices requiring low LO power, to determine the HEB's sensitivity. The LO power requirement (Sec. IV C) should be low enough in view of the limited available LO power that can be coupled to the HEB. Furthermore, a sufficiently large IF noise bandwidth (Sec. IV D) is relevant since it enables the instantaneous observation of signals that are relatively wide or separated far in IF frequency. Finally, to achieve a reasonable signal to noise ratio, the IF signal generally has to be integrated over a very long period. The required integration time decreases quadratically[21,22] with lower T_N.

The paper is organized as follows. In Sec. II we discuss the device's fabrication, dc characterization, and the evaluation of the twin-slot antenna. In Sec. III we describe the setup. In Sec. IV we discuss the selection of measured mixer properties and end in Sec. V with conclusions.

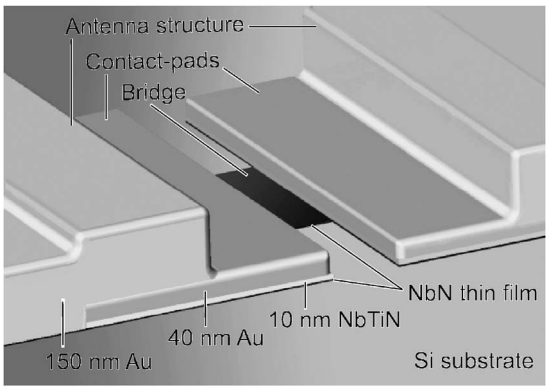

FIG. 1. Sketch of the HEB structure. It shows the NbN bridge in between the contact pads which consist of 10 nm NbTiN and 40 nm Au. Also shown is (part of) the 150 nm thick Au antenna layer on the NbN film and partly on the contact pads.

II. TWIN-SLOT ANTENNA COUPLED SMALL AREA NBN HEB

A. Fabrication

The HEB device under consideration is based on a NbN superconducting film that is sputter deposited on a high purity Si substrate at the Moscow State Pedagogical University in Moscow.[16] The film thickness is expected to be 3.5 nm from the deposition rate. We note, however, that transmission electron microscope (TEM) inspections suggest that the actual thickness is around 5.5 nm. The unprocessed NbN film has a critical temperature (T_c) of 9.3 K.

A sketch of the HEB structure is shown in Fig. 1. The antenna is connected to the NbN film by contact pads consisting of 10 nm NbTiN and 40 nm Au on top. The contact pads are fabricated by cleaning the NbN surface followed by *in situ* sputter deposition of the metal layers. The precise contacting to the NbN film by the contact pads turns out to be essential for the mixer performance of HEBs.[12] These insights are examined process- and modelwise elsewhere.[23,24] The antenna is defined by liftoff using a negative e-beam resist mask and *in situ* evaporation of 5 nm Ti for adhesion, 150 nm Au, and on top 10 nm Ti to avoid redeposition of Au during later etch steps. As a last step, the bridge width is defined between the contact pads by a negative e-beam resist etch mask and subsequent reactive ion etching. The final dimensions of the small area NbN HEB are 150 nm long and 1 μm wide. After fabrication, the remaining 300 nm thick e-beam resist etch mask is left on top of the HEB bridge. A scanning electron microscope (SEM) micrograph of this device is shown in Fig. 2 and in close-up in Fig. 3 as an inset.

B. dc characterization and analysis

Here we discuss all dc properties that can be used as performance indicators to verify the quality of devices. We focus on one device which has thoroughly been analyzed. We find that devices with similar dc properties provide simi-

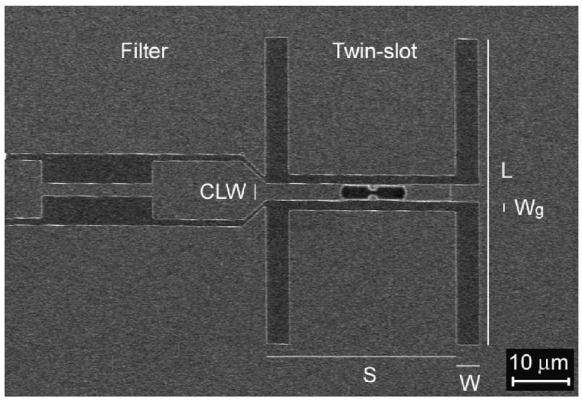

FIG. 2. SEM picture showing a top view of the twin-slot antenna coupled HEB mixer and part of the filter structure. The dark structure in the center of the twin slot is the remaining e-beam resist used as an etching mask for the NbN bridge. The antenna is designed for a center frequency of 1.6 THz. Relevant parameters are marked by white bars.

lar performance (to within 10%) and we therefore believe that our analysis is representative. The device resistance versus temperature (RT) curve is shown in Fig. 3 on a logarithmic scale. Derived from the normal state resistance at 16 K ($R_{16\ \mathrm{K}}$), the square resistance ($R_{\square,16\ \mathrm{K}}$) is ~900–1000 Ω.[23] Measurements on similar structures with varying length confirm this value. The $R_{\square,16\ \mathrm{K}}$ determines the aspect ratio of the bridge because of the HEB's impedance requirement for optimal antenna matching (~110 Ω). The RT curve shows three clear superconducting transitions. The lowest transition ($T_{c,a}$) is due to the proximitized NbN under the whole antenna structure (see Fig. 1). The middle transition ($T_{c,\mathrm{stack}}$) is associated with the total stack layer of the contact pads and the NbN film. The highest transition ($T_{c,\mathrm{bridge}}$) is due to the NbN bridge itself.[26] Here $T_{c,\mathrm{bridge}}$ is defined as the temperature at which the resistance reaches half the value of $R_{16\ \mathrm{K}}$.

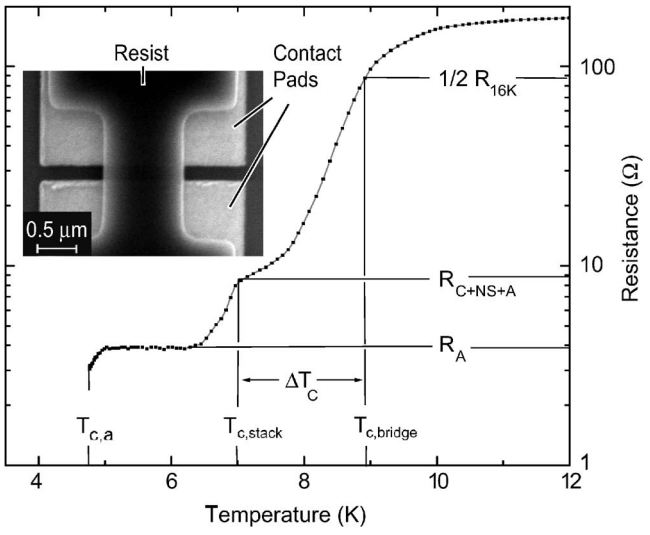

FIG. 3. Resistance vs temperature of the small area HEB. $R_{16\ \mathrm{K}}$ is the normal state resistance at 16 K, R_A the normal state resistance of the antenna, $R_{C+\mathrm{NS}}$ the resistance just above $T_{c,\mathrm{stack}}$ with $T_{c,\mathrm{stack}}$ the critical temperatures of the stack layer consisting of the NbN film with contact pad on top, $T_{c,a}$ the critical temperatures of the antenna, and $T_{c,\mathrm{bridge}}$ the critical temperatures of the NbN bridge, defined at $\frac{1}{2}R_{16\ \mathrm{K}}$. Inset: zoomed SEM micrograph of the HEB bridge between the contact pads covered by an e-beam resist layer.

The $T_{c,\mathrm{stack}}$ is lower than the $T_{c,\mathrm{bridge}}$ as a result of the superconducting proximity effect between the superconducting NbN and the contact pad's Au/NbTiN bilayer. Hence the transparency of the interface between NbN and contact pad will affect the difference $\Delta T_c = T_{c,\mathrm{bridge}} - T_{c,\mathrm{stack}}$. Because the NbTiN/Au bilayer has a different (lower) T_c than $T_{c,\mathrm{bridge}}$, a more transparent interface yields a larger ΔT_c. We empirically find that for the device to have good mixer performance, the optimal ΔT_c is about 2 K.

Our contacting procedure also aims to minimize the contact resistance (R_C) that is commonly reported for HEBs fabricated without additional cleaning process of the contacts. Reducing the contact resistance is important since we experimentally find that a R_C that amounts to a significant fraction of the bridge resistance leads to deteriorated device performance, likely due to RF dissipation under the contacts not contributing to the mixing. For the small area (narrow) device, obviously the influence of R_C becomes more prominent.

Yet, even for fully clean interfaces at temperatures T for which $T_{c,\mathrm{bridge}} > T > T_{c,\mathrm{stack}}$ the dc resistance of the contacted superconducting bridge is nonzero due to normal-to super- (NS) current conversion from the normal contact pads to the superconducting bridge.[25] The consequence is that there will be a resistive contribution at each NS interface over about one coherence length ξ (~3 nm in NbN) even for fully clean interfaces. Besides this there is also a (small) series resistance (R_A) originating from the IF output line, the filter, and the coplanar waveguide transmission (CPW) line between the two slots (see Fig. 2).

We estimate the real contact resistance from $R_C = R_{C+\mathrm{NS}+A} - R_{\square,16\ \mathrm{K}}(2\xi/W_{\mathrm{bridge}}) - R_A$, in which $R_{C+\mathrm{NS}+A}$ is the device resistance just above $T_{c,\mathrm{stack}}$ and W_{bridge} the width of the HEB bridge. We find that for the device under consideration the R_C is negligible (<1 Ω), so that $R_{C+\mathrm{NS}+A}$ can largely be ascribed to the NS conversion on either side into the NbN bridge and the antenna resistance. Note that a "hidden" contribution of the contact resistance to $R_{\square,16\ \mathrm{K}}$ can be excluded based on extrapolating the resistance of narrow HEB-like devices with varying length.[23] It is worth pointing out that the analysis of the RT curve is necessary for each new batch as R_C is highly sensitive to the details of the processing.

Another important property extracted from Fig. 3 is the measured $T_{c,\mathrm{bridge}}$ of the NbN bridge of ~9 K. The $T_{c,\mathrm{bridge}}$ influences the IF bandwidth since it sets the approximate electron temperature under operation.

We note that the (dc) properties of the HEB are sensitive to aging in normal atmosphere without the use of a passivation layer.[27] The device under consideration lacks such a layer. However, this device is kept in vacuum to avoid aging and, as a result, shows no significant changes in dc parameters during the course of the whole characterization.

C. Antenna design and evaluation

The NbN HEB is coupled to a quasioptical twin-slot antenna designed for a center frequency of 1.6 THz. Specifically, we choose the following dimensions[29] (assuming a Si

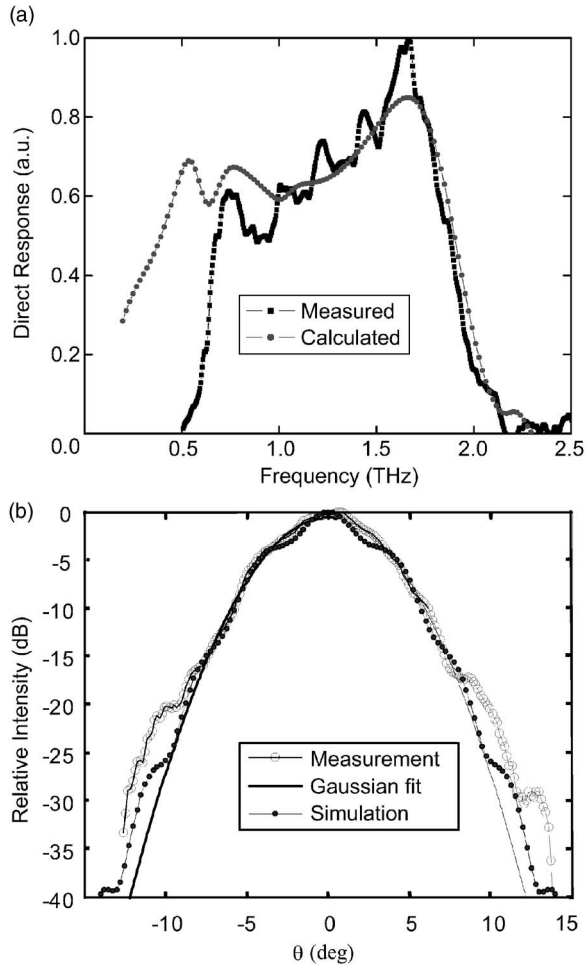

FIG. 4. (a) Normalized direct response of the twin-slot antenna coupled HEB mixer measured (corrected for optics) with a Fourier-transform spectrometer. The calculated response (normalized) is also included for comparison. (b) Measured (normalized) and calculated beam pattern (*H*-plane) and fundamental mode Gaussian fit of the uncoated antenna-lens combination at 1.2 THz.

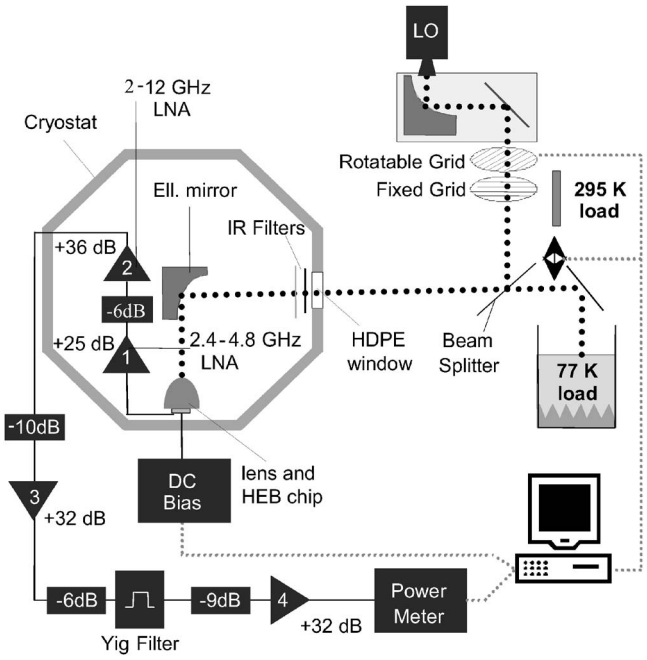

FIG. 5. Schematical picture of the experimental setup.

substrate), illustrated in Fig. 2: the slot length L is $0.30\lambda_0$ with λ_0 the free space wavelength. The slot separation S is $0.17\lambda_0$, the slot width W is $0.07L$. The CPW impedance transformer has a central line width (CLW) of 2.8 μm and a gap W_g of 1.4 μm, yielding a characteristic impedance of 51 Ω.[30] To avoid leakage of the RF signal via the IF output line, a RF choke filter is used with three sections each consisting of one high (70 Ω) and one low impedance (26 Ω) segment, each being a quarter wavelength (18.7 μm) long. Based on this, we predict a maximum power coupling efficiency from the antenna to the HEB bridge[29] of 88%–90% at 1.6 THz, depending on the precise bridge resistance in the optimum range between 100 and 150 Ω.

The experimental evaluation of the antenna response and beam pattern is performed using the HEB chip with a thickness of 335 μm glued to the center of an elliptical Si lens without antireflection (AR) coating. The lens has a diameter of 5 mm, an ellipticity of 1.0193, and an extension length of 0.756 mm. The antenna-lens combination is evaluated with an evacuated Fourier-transform spectrometer (FTS).

Figure 4(a) shows the antenna response of the mixer measured in the FTS, after correction for the frequency dependent transmission of the beamsplitter of the FTS, the window, and the heat filter of the cryostat. In the same figure we show the simulated response. The maximum direct response coincides with the design frequency at 1.6 THz and follows the simulated response rather well, except for a small deviation at the lower frequency end.

In addition, we evaluate the beam pattern of the mixer at 1.2 THz and compare it to calculations using the software package "PILRAP."[31] We mount the antenna-lens combination, described previously, in the cryostat as close as possible to the window. The far-field phase and amplitude pattern of the antenna-lens combination are measured without any intermediate optics in a heterodyne detection mode using a 1.2 THz solid state direct multiplied LO source and a Schottky harmonic generator driven at 200 GHz as the RF source (Fig. 5). By using the narrow-band homodyne detection technique reported by Jellema *et al.*[32] we obtain a signal-to-noise ratio of more than 60 dB. Figure 4(b) shows the measured far-field beam pattern (*H* plane) of the double-slot antenna-lens combination at 1.2 THz. The general structure of the far-field pattern is fairly well predicted by PILRAP. The overall shape is gaussian apart from some structures in the upper 5 dB and shoulders appearing at typically −20 dB. The measured gaussicity, evaluated as the normalized complex overlap integral between the measured field and a fundamental mode gaussian,[33] is found to be 93%. The measured, predicted, and fitted beam width at the −10 dB level agree within 5%. The shoulders are seen both in the measured and predicted patterns but appear at lower levels for the latter. The differences might originate from simplifications in the PILRAP calculation or incorrect assumptions on the LO horn. The main outcome of this beam pattern evaluation is that the measured and predicted beam width agree well to first order. However, in this configuration the location of the phase center of the antenna-lens combination cannot

TABLE I. Optical losses in the LO path measured at 1.5 THz.

Element	Gain (dB)
Antenna-lens combination	−0.5
Lens reflection (coated)	−0.1
Three Zytex heat filters	−0.6
HDPE window	−0.7
3.5 μm splitter	−15
Air 20 cm 40% relative humidity (RH)	−0.2
Double grid maximum transmission	−0.9

be measured with more accuracy than 2–3 mm. Jellema *et al.*[32] reported that the phase center can differ several millimeters as compared to the predicted position. In fact, a more recent measurement on an identical lens at 1.6 THz with AR coating has revealed that the actual phase center is shifted back by 1.5 mm with respect to the vertex of the lens. This was unknown at the time of the optical design and manufacturing. Obviously this has consequences for the LO coupling, which we will analyze in Sec. IV C.

III. MEASUREMENT SETUP

The full characterization of the HEB as a heterodyne receiver is performed by using a dedicated quasioptical setup. The optics available for the setup is designed based on measurements of the antenna and LO beam to optimize the coupling between LO and HEB. Furthermore it provides fast and reliable data taking by fully automating the measurements.

The diagram of the complete setup is depicted in Fig. 5. The LO source is a solid state of 1.45–1.55 THz multiplier chain.[4] The chain is operated at 1.46 THz where it has a peak output power of 11 μW, evaluated using a calibrated Neil-Erickson power meter[34] and independently with a Thomas-Keating power meter.[35] The output of the LO is equipped with a diagonal feed-horn designed for 1.6 THz. Directly in front of the LO is a two mirror system, consisting of a focusing ellipse and a flat, mounted firmly on a *XYZ* stage on a second optical parallel rail. Next, the LO beam encounters a double grid system consisting of a computer controlled wire grid and a fixed wire grid with a vertical polarization. Because the LO is vertically polarized each grid attenuates the power by a factor of $\cos^2(\phi)$. The two grids, one after the other, give an expected total attenuation of $\cos^4(\phi)$. This has been confirmed experimentally, ruling out significant influence of the diagonal horn on the LO beam polarization. After the grids the signal is coupled reflectively into the cryostat by a 3.5 μm Mylar beam splitter. For the cryostat, we use a 0.9 mm high density polyethylene (HDPE) sheet as vacuum window, one layer of Zytex G104 at 77 K and two identical layers at 4.2 K as infrared filters. A focusing mirror is used to match the beam from the lens with the beam coming in from the cryostat window. The lens is identical to the one used in Sec. II C except that it is coated with a 29 μm thick layer of Parylene-C as antireflection coating optimized for 1.6 THz.

The transmitted power fraction from the LO horn to the front of the HEB mixer lens is given by $0.017\cos^4(\phi)$ (see Table I). The main loss is due to the beam splitter (~97% loss), which in practice can be decreased by using a (Martin-Puplett) interferometer with less than ~10% loss. The loss from the lens surface to the HEB chip amounts to −0.6 dB.

We measure the *Y* factor by alternating a 295 K hot load and a 77 K cold load with a chopper at ~10 Hz. This signal is transmitted through the beam splitter (0.08 dB loss), where it is combined with the LO signal and both follow the same path into the cryostat as described before. The air path between either the calibation loads or the LO horn to the cryostat window is in both cases of the order of 20 cm and the relative humidity is ~40%. The total signal loss from the hot/cold load to the HEB at the LO frequency is ~−2.2 dB (see Table I). The effective temperatures of the hot and cold loads at the mixer chip calculated using the Callen and Welton limit[36] are 208 and 114 K, respectively. The total power difference between the hot and cold loads evaluated at the HEB is estimated to be 1.2 nW. This value is calculated taking into account the frequency dependent losses of all optical elements within the antenna bandwidth determined by FTS in Fig. 4(a).

The lens-HEB combination is placed in a mixer block with internal bias *T* and is thermally anchored to the 4.2 K plate of the cryostat. The IF output of the mixer unit is connected to a 10 cm long semirigid Al SMA cable to the input of the first low noise amplifier (LNA).[37] Because of its low gain this amplifier is connected to a second cryogenic LNA.[38] The signal is further amplified at room temperature, routed to a yttrium iron garnet (YIG) filter with a 50 MHz bandwidth, and detected using a commercial power meter. Care was taken to assure linearity of the whole chain.

IV. EXPERIMENTS

A. Receiver noise temperature

In Fig. 6(a) the uncorrected double sideband receiver noise temperature (T_N) of the mixer over a broad range of bias points is shown. Each bias point is uniquely defined by the bias voltage *V* and local oscillator (pumping) power P_{LO}. For a fixed bias voltage, the bias current reflects the level of LO pumping. We obtain T_N based on the measured *Y* factor using the Callen and Welton definition.[36] The measurement is performed at the IF frequency that yields the best sensitivity, experimentally found to be F_{IF}=2.8 GHz (see Fig. 9). We observe a relatively broad bias range of optimal response centered around a bias voltage of 0.5 mV with a maximum sensitivity of T_N=900 K. This proves that the small area HEB can successfully be operated in combination with the solid state LO at 1.5 THz. Also, at low bias voltages and high currents a small area with unusually low T_N can be seen in Fig. 6(a). This will later be shown to be an artifact of the direct detection effect.

B. Direct detection

HEBs can exhibit direct detection in addition to heterodyne response in a standard hot/cold load measurement.[40] It becomes prominent when the RF power from the calibration load absorbed in the bridge is non-negligible compared to the absorbed LO plus dc power. In the case of our small area HEB the P_{LO} at optimal operating point absorbed in the

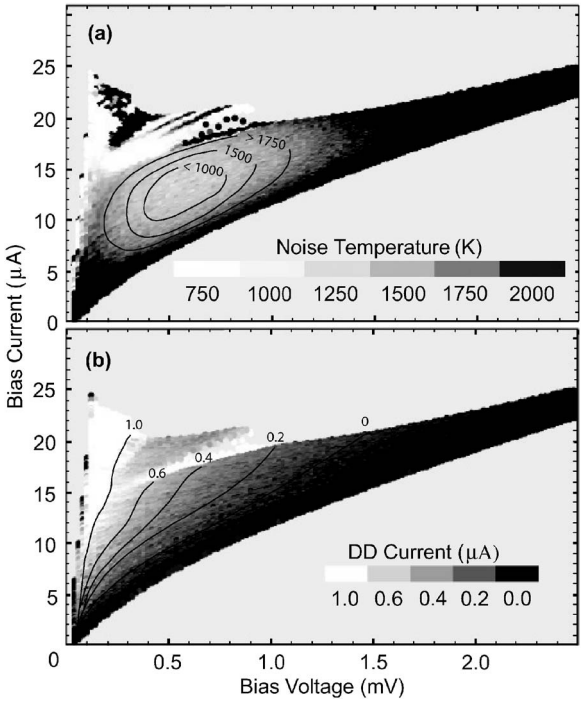

FIG. 6. (a) Uncorrected double sideband receiver noise temperature T_N at an LO frequency of 1.46 THz in a two-dimensional plot of voltage vs current. The latter is a function of the applied LO power. The minimum value is T_N=900 K. Contour lines indicate absolute values of T_N. (b) The direct detection current $I_{DD}=I_{hot}-I_{cold}$ in a two-dimensional plot of voltage vs current. Contour lines indicate absolute values of I_{DD}.

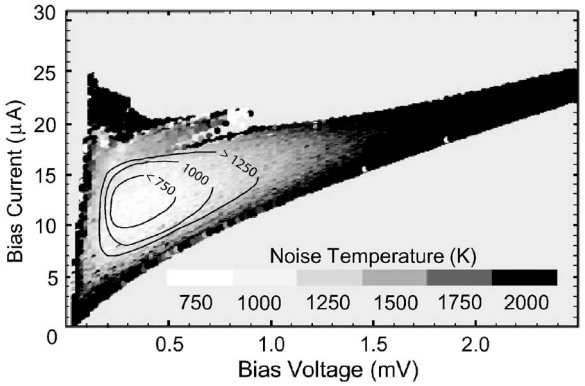

FIG. 7. The double sideband receiver noise temperature at 1.46 THz in the small signal limit, $T_{N,S}$. The minimum value of $T_{N,S}$ is 700 K. The contour lines indicate absolute values of $T_{N,S}$.

bridge is 25 nW (from Sec. IV C). The dc bias voltage for optimum T_N is centered around 0.5 mV, with a dc bias current around 10 μA leading to an absorbed dc power P_{dc} of ~5 nW. The total calibration-load power difference when switching from the 77 to 295 K load is ~1.2 nW (see Sec. III). This is large enough compared to the 30 nW ($P_{LO}+P_{dc}$) to noticeably change the bias point of the mixer, which expresses itself as the decrease in bias current (the bias voltage is also monitored and remains unchanged) when switching from the 77 to 295 K load. As a result we evaluate the hot load output power at a slightly lower bias current than the cold load output power. Because the mixer output power is a function of bias current, the Y factor is influenced by the bias current shift and hence an error is introduced into the calibration procedure for T_N.[40]

We now address what the consequences of the direct detection are for operating the HEB as receiver in a heterodyne spectrometer. The (astronomical) RF source represents itself as small narrow line features with negligible integrated total power on top of a background with an identical power input as the "off" source measurement, e.g., consisting of a piece of (cold) sky. Thus, switching between "on" to off source results in a negligible value of I_{DD}. This implies that although in principle the direct detection effect is absent for the astronomical observation itself, it can affect the absolute power calibration (e.g., using the 295 K "hot" and 77 K "cold" loads).

To quantify the direct detection effect we measure the bias current I_{hot}/I_{cold} at hot/cold load during the Y factor measurement. We show in Fig. 6(b) the measured direct detection current, defined as $I_{DD}=I_{hot}-I_{cold}$. The magnitude of the direct detection current ranges from about 0 μA at high bias voltages to more than −1 μA at very low bias voltages. We observe that I_{DD} is always negative in agreement with results reported previously.[40,41] It indicates that the difference in RF power between the 77 and 295 K load changes the bias current of the mixer in the same way as an increase in P_{LO}.

This implies that to correct the direct detection we have to reduce P_{LO} when switching from cold to hot load to make sure that the bias current remains constant, thus compensating for the bias current shift. In essence the compensation makes the *real* bias point that is defined by the LO+RF power and bias voltage identical for both hot and cold loads. We perform this recalibration *after* the measurement by constructing a two dimensional plot of the receiver output power at hot load and at cold load as a function of bias voltage and current. From these two maps we evaluate the small signal Y factor, from which we obtain the noise temperature in the small signal limit ($T_{N,S}$), as shown in Fig. 7. We find a minimum value of $T_{N,S}$=700 K, which is 22% lower than the minimum value of T_N=900 K. We also observe that the location of the minimum in the noise temperature is shifted to lower bias voltages. Also, the area with the low noise temperatures at small bias voltages in Fig. 6(a) has disappeared after the correction. The conclusion is that the optimum sensitivity is underestimated by 20% by the standard Y factor method.

The direct detection implies a complication in any instrument calibration. The only way to avoid recalibration is to minimize the total power difference between the hot and cold loads, e.g., by reducing the RF bandwidth. This can be achieved by either using a narrow RF bandpass filter in the signal path at the cost of a slight loss or the use of a waveguide. Another method to diminish the power difference is the reduction of the temperature difference between the calibration loads. To confirm this idea we essentially repeated the experiment with a metal mesh narrow RF bandpass filter[42] mounted in front of a slightly different HEB mixer at the 4.2 K stage of the cryostat. The filter has a center frequency of 1.6 THz, at which the loss is only −0.2 dB, and has an effective bandwidth of 200 GHz. Hence the filter reduces the effective RF input bandwidth of the receiver by a

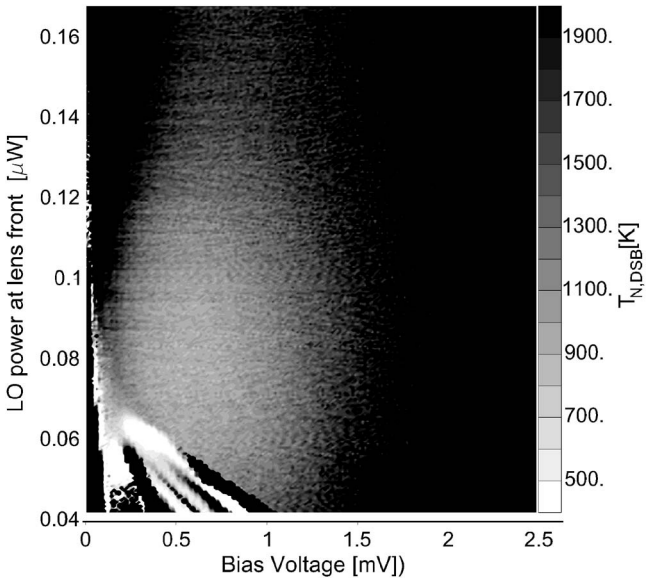

FIG. 8. Uncorrected double sideband receiver noise temperature at 1.46 THz in a two-dimensional plot of bias voltage vs the estimated LO power at the lens front of the mixer unit.

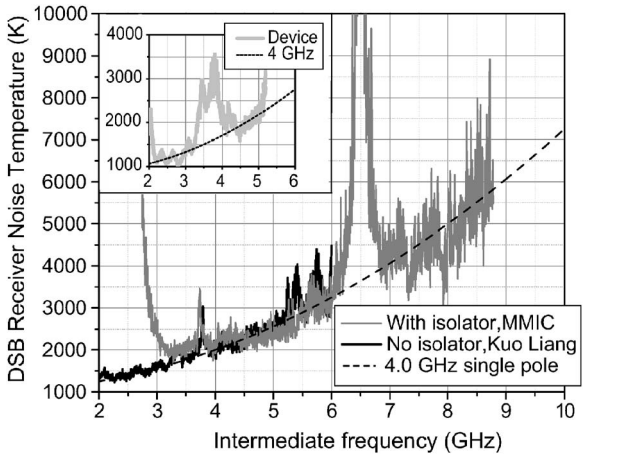

FIG. 9. DSB receiver noise temperature as a function of IF frequency at 1.46 THz at the optimal operating point of the mixer. Dark gray line: using the MMIC LNA (by Weinreb) and isolator. Black line: Without the isolator but with the Kuo-Liang LNA. The dotted line represents a single pole roll-off at 4 GHz, with T_N at zero frequency of 1000 K. Inset: Original noise bandwidth measurement (gray line) of the actual device but using the old design bias board and a single pole roll-off at 4 GHz (black dotted line).

factor of 4.5. As a consequence the power difference between the hot and cold loads is 0.2 nW, only 0.4% of the isothermal $P_{\mathrm{LO}}+P_{\mathrm{dc}}$ of ~65 nW. We find a minimum noise temperature of $T_N=700$ K measured at LO frequency of 1.6 THz,[43] that is 15% lower than the T_N without the use of the filter ($T_N=800$ K). It is interesting to realize that the best T_N we find is identical to the best sensitivity of 700 K reported in a spiral-antenna coupled, large area ($4.0\times0.4\ \mu\mathrm{m}^2$) HEB mixer[12] at the same frequency.

C. LO power requirement

We evaluate the required LO power using two independent methods. First we use the isothermal technique[39] to find the P_{LO} that is absorbed in the bridge by applying it to the measured current-voltage (*IV*) characteristic of the HEB at high bias. The method is based on the assumption that the effect of RF and dc powers on the *IV* is equivalent. Using this "bottom-up" procedure we find a P_{LO} of 25 nW at optimal P_{LO}.

Second we determine the LO power based on the calibrated LO output power and the known optical losses. The latter approach yields the fraction of the total LO power coupled to the HEB mixer, equal to $0.015\cos^4(\phi)$ (see Table I). Using the known grid angle ϕ and accurately known LO output power this "top-down" approach allows us to plot the noise temperature as a function of P_{LO} (see Fig. 8). At optimal pumping level the P_{LO} corresponds to 80 nW at the lens front and an estimated 60 nW at the mixer. The latter is the actual LO power incident on the HEB chip. Hence there is a factor of 2.3 difference between the actual LO power dissipated in the HEB and the LO power incident on the HEB chip.

To confirm this difference we first verify the accuracy of the isothermal technique using the direct detection effect described in Sec. IV B. We focus on the shift in the *IV* curve due to direct detection when switching between the hot and cold loads. By applying the isothermal technique we find a difference in absorbed power in the mixer between hot and cold loads of 1.4 ± 0.1 nW. This value is in agreement with the calculated power difference of 1.2 nW described in Sec. III. A nearly "one to one" correspondence between isothermal technique and real LO power has also been reported for waveguide HEB mixers.[44]

The observed difference between LO powers in our experiment may thus be caused by imperfect beam matching between the LO source and the antenna-lens combination. To verify this, detailed LO coupling calculations have been performed based largely on the experimental characterizations discussed in Sec. II C. In particular, the offset in phase center, the actual field distribution of the antenna-lens combination and diagonal horn, and the polarization efficiencies are taken into account in evaluating the full overlap integral. The analysis of our optical layout yields a maximum LO coupling of $50\pm10\%$. This corresponds to a factor 2 ± 0.4 difference between incident and absorbed LO power in the HEB. Imperfect beam matching thus fully explains the observed difference. Hence we confirm that the isothermal technique is a correct method to determine the LO power absorbed in a HEB. We have to stress that it is very difficult to experimentally realize a LO-HEB coupling close to 100%, and that the same argument applies to the signal beam coupling defined by the telescope optics in a practical receiver. However, using the insights gained by this analysis, one can optimize the design (e.g., with corrected phase center) to improve the beam coupling efficiency up to ~75%.

D. IF bandwidth

To determine the IF noise- and gain-bandwidth we measure, at the optimum operating point of the mixer, the hot and cold load output powers as a function of the YIG-filter center frequency. In the inset of Fig. 9 the measured noise performance versus IF frequency is plotted. This bandwidth measurement was performed with an IF circuit board that does

not allow a correct evaluation of the mixer properties at frequencies beyond ~5 GHz (see the inset of Fig. 9). We therefore focus on the measurement using a different IF circuit board and mixer block, which happened to be available with a similar HEB mixer, however, with a lower $T_{c,\mathrm{bridge}}$ of 8.4 K.

We use a basic IF board that only forms the transition between a CPW at the HEB chip and a SMA launcher at the other end. An external Miteq bias *T* is used to enable mixer biasing. After the bias *T* we use a Pamtech 3–10 GHz cryogenic isolator followed by the first LNA.[38] The rest of the setup is similar to what we described before. To evaluate the IF noise at lower IF frequencies we also measured it without the isolator using the amplifier chain of our standard setup described in Sec. III.

The measured frequency dependence of the receiver noise temperature is shown in Fig. 9. Except for the resonance at ~6.5 GHz, the new IF circuit board behaves well at the higher frequencies. At lower frequencies the measurements were performed without the isolator providing excellent data, which are also plotted in Fig. 9. The complete frequency dependence of the noise shown in Fig. 9 can be fitted to first order by a 4 GHz single pole roll-off. The extrapolated T_N at zero frequency is 1000 K. We note that at low frequencies the frequency dependence of T_N looks very similar to the one measured with the original IF circuit board and device (see the inset of Fig. 9).

The single sideband mixer gain $G^{\mathrm{cw}}_{\mathrm{mix,SSB}}$ is also determined from the *Y*-factor measurement using

$$G^{\mathrm{cw}}_{\mathrm{mix,SSB}}(f) = \frac{\Delta P_{out}}{2\mathrm{BW}_{\mathrm{IF}} k_B G_{\mathrm{IF}} (T^{\mathrm{cw}}_{\mathrm{in,hot}} - T^{\mathrm{cw}}_{\mathrm{in,cold}})}, \quad (1)$$

in which ΔP_{out} is equal to the difference in IF output power between hot and cold loads, G_{IF} the gain of the IF chain, k_B Boltzmann's constant, and $\mathrm{BW}_{\mathrm{IF}}(f)$ the YIG-filter bandwidth. A correct evaluation of $G^{\mathrm{CW}}_{\mathrm{mix,SSB}}$ is only possible when all the parameters of the above equation are known, especially the frequency dependence of the gain of the IF chain. We calibrate the gain by measuring the IF output power as a function of frequency for several temperatures of the mixer between 15 and 35 K. Since the HEB mixer acts in this temperature range as a thermal load with a resistance of 175 Ω, we know the exact thermal noise power at the input of the IF chain. We can therefore use this measurement to calibrate the IF chain. By this procedure we neglect, however, the effect of different (frequency dependent) impedance matchings of the HEB under operating conditions. We find an IF chain noise temperature of about 10 K, which is higher than the amplifier noise due to the noise from the isolator and the impedance mismatch between the HEB and the isolator. The gain is approximately 94 dB at 2 GHz, which slowly decreases to 80 dB at 9 GHz. As a control measurement we also measure the total gain of the warm part of the chain using a vector network analyzer. Adding to this measurement the known gain of the cryogenic LNA gives an IF circuit gain virtually identical to the one obtained from the calibration measurement using the HEB mixer as a thermal load. We note that the frequency dependencies of the SMA cables have been neglected, justified by room temperature transmission measurements using a vector network analyzer.

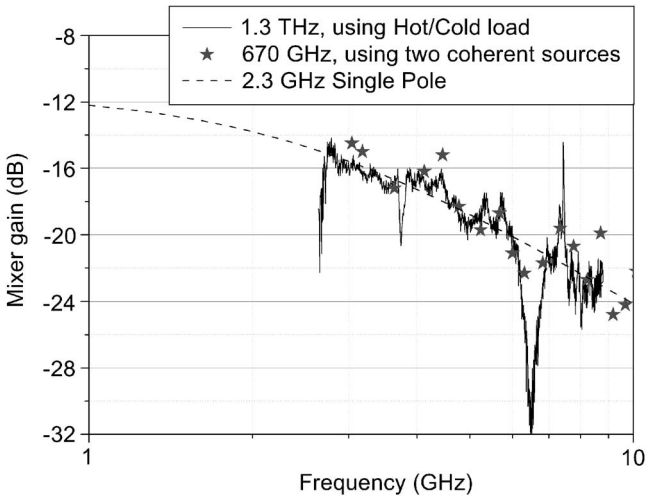

FIG. 10. Mixer gain bandwidth obtained at 1.46 THz using the Weinreb MMIC LNA and a hot/cold load technique. Asterisk symbols: Mixer gain bandwidth at 670 GHz measured using two coherent sources. The dotted line represents a single pole fit with a roll-off at 2.3 GHz.

The measured frequency dependence of the mixer gain is shown in Fig. 10. Moreover, in the same figure we show by the asterisk symbols, a direct measurement of the relative conversion gain at 670 GHz using two coherent sources, one as LO and the other as the RF signal. Within the error bars both data sets overlap nicely. Also shown is a first order fit to a single-pole roll-off curve. The −3 dB gain bandwidth is 2.3 GHz. This value is lower than the bandwidth observed for HEBs based on a similar NbN film.[12,14] The lower value is likely due to the reduction of $T_{c,\mathrm{bridge}}$ to 8.4 K because of an additional baking process applied to this particular HEB.[43] The lower $T_{c,\mathrm{bridge}}$ can reduce, e.g., the electron-phonon interaction and thus result in a longer thermal time constant, in turn leading to a reduced IF bandwidth. Note that higher bandwidths up to 6 GHz are observed at high bias voltages. The latter can be interpreted as a result of the higher electron and phonon temperatures in the bridge due to the large (dc) power dissipation.

The measured ratio of the noise bandwidth with the gain bandwidth at optimal bias, $f_N/f_G = 1.7$, can be compared to a theoretical estimate based upon the analysis used by Karasik and Elantiev[45] and Cherednichenko *et al.*,[46] where it is found that $f_N/f_G = \sqrt{[T_{\mathrm{out}}(0)+T_{\mathrm{IF}}]/[T_J(0)+T_{\mathrm{IF}}]}$. Here $T_{\mathrm{out}}(0)$ is the mixer output noise of the mixer at low IF frequencies, 45 K in our case, $T_J(0)$ the mixer Johnson noise, which is approximately equal to $T_c = 9$ K and $T_{\mathrm{IF}} = 10$ K the IF chain noise temperature. Thus we find a "theoretical" value of $f_N/f_G = 1.7$, which is in good agreement with the measurement.

E. Stability

We characterize the stability of the mixer at the optimal operating conditions by measuring the Allan variance[47] of the receiver. The Allan variance is defined as $\sigma^2_A(t) = \frac{1}{2}\sigma^2_D(t)$, where $\sigma^2_D(t)$ is the variance of the difference of contiguous measurements of duration *t*. The noise of any receiver system is a combination of three terms: white (uncorrelated) noise, $1/f$ electronic noise and low frequency drift noise.

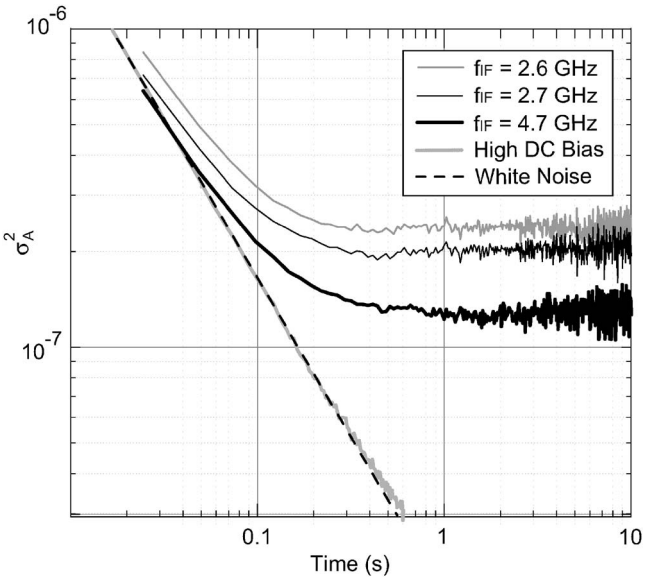

FIG. 11. Continuum Allan variance of the small area NbN HEB receiver operated at 1.46 THz obtained in a 50 MHz bandwidth around 2.6, 2.7, and 4.7 GHz. The theoretical white noise behavior and stability behavior of the HEB driven into normal state by high dc bias are included for comparison.

The latter two cause the system's instability. From a mathematical analysis it can be shown that the Allan variance for a noise spectrum containing all three noise contributions is given by

$$\sigma_A^2(t) = \frac{a}{t} + bt^{\beta} + c, \tag{2}$$

where a, b, c, and β are constants and t is the integration time. The Allan variance can thus be used as a tool to discriminate between different noise terms. For a short integration time, the first term in the above equation dominates and the Allan variance decreases as $1/t$, as expected for white noise. For a longer integration time, the drift will dominate as shown by the term at^{β}. In that case, σ_A^2 starts to increase with the power β, which is experimentally found to be between 1 and 2. On other occasions, it is observed that the variance levels off at some constant value. This is attributed to the constant factor c in Eq. (2) and is representative of flicker or $1/f$ noise in the electronics. Plotting $\sigma_A^2(t)$ on a log-log scale demonstrates the usefulness of this approach in analyzing the noise statistics. The minimum (or start of a horizontal slope) gives the "Allan" time (T_A), at the crossover from white noise to drift or $1/f$ noise.

To avoid drift and $1/f$ noise from dominating, one must keep t below the system's Allan time. For the sake of optimum integration efficiency one has to limit t even further where σ_A^2 still closely follows the white noise behavior.

We performed the Allan variance measurement of the receiver system by monitoring the IF output power as a function of time. Note that it is vital to use signal powers of at least −10 dBm within the YIG-filter bandwidth. This is to ensure that one measures the mixer properties by the wideband power head instead of the noise statistics out of the YIG-filter band. In Fig. 11 we show the Allan variance taken at the optimal operating conditions. In a single (continuum) 50 MHz wide channel, the mixer stability curves already deviate about one order of magnitude at 0.2–0.3 s from the integrated white noise. The stability behavior is very similar (except the absolute variance) for various IF frequencies at 2.5, 2.7, and 4.7 GHz. Also in Fig. 11 is the $\sigma_A^2(t)$ while operating the HEB in the normal state by applying a high dc bias (10 mV), where the HEB is essentially a white noise source (no mixing). The measured Allan time of several seconds shows that we can exclude the instabilities in the IF chain as a dominant factor.

To further distinguish between the role of the HEB itself on the stability and other contributions we repeat the Allan variance measurement at 675 GHz and subsequently replace the HEB mixer by a waveguide superconductor-insulator-superconductor (SIS) mixer designed for ~700 GHz. SIS mixers are known to have a much longer Allan time. We find an Allan time of several seconds for the SIS receiver. The latter identifies the HEB mixer as the limiting factor for the stability. The physical reason for the instability of the HEB is still not clear, but is likely related to the random (thermal) modulation of the mixing region in the bridge. We note that the measured stability of the small area device is similar to that of our large area (4.0×0.4 μm^2) device.[48] This is different from other reported results,[49] in which the smaller area HEBs demonstrate a shorter Allan time.

V. CONCLUSIONS

We demonstrate a heterodyne terahartz receiver system based on a small area NbN HEB in combination with a solid state tunable LO source. The full analysis of the receiver reveals all relevant mixer parameters related to the performance of the HEB. The measured sensitivity is excellent judging by the uncorrected double sideband (DSB) receiver noise temperature of 900 K at 1.46 THz. The required LO power in the NbN bridge, determined by the isothermal technique, is 25 nW whereas the required LO power incident on the HEB chip is 60 nW. The difference is due to the imperfect beam matching between the LO source and antenna-lens combination. The considerably low LO power requirement allows the operation of an HEB in combination with a state-of-the-art solid state LO sources up to ~2 THz. Due to the low LO power in combination with the wide RF bandwidth of the twin-slot antenna, a correction for direct detection is necessary. For our specific receiver system this leads to a DSB receiver noise temperature of 700 K. The IF gain bandwidth is 2.3 GHz and the noise bandwidth is 4 GHz. The continuum stability based on measurements of the Allan variance is of the order of 0.3 s in a 50 MHz bandwidth. This stability is adequate for certain applications, allowing line surveys in chopped mode. However, continuous observations are likely impossible. Finally, an offshoot of our analysis is that the isothermal technique is confirmed to be a correct method to determine the LO power at the HEB.

ACKNOWLEDGMENTS

We thank B. Voronov and G. Gol'tsman for providing us with the NbN films, JPL for making available the tunable

solid state LO chain for our experiment, and the help of J. Kawamura thereby. The work is supported financially by the EU through RadioNet and INTAS program.

[1]J. W. Waters *et al.*, IEEE Trans. Geosci. Remote Sens. **GE–44**, 1075 (2006).
[2]P. H. Siegel, IEEE Trans. Microwave Theory Tech. **50**, 910 (2002).
[3]J. Zmuidzinas and P. L. Richards, Proc. IEEE **92**, 1597 (2004).
[4]A. Maestrini *et al.*, IEEE Microw. Wirel. Compon. Lett. **14**, 253 (2004).
[5]R. Köhler *et al.*, Nature (London) **417**, 156 (2002).
[6]J. R. Gao *et al.*, Appl. Phys. Lett. **86**, 244104 (2005).
[7]T. Gaier *et al.*, in *Proc. Far-IR, SUB-MM & MM Detector Technology Workshop*, edited by J. Wolf, J. Farhoomand, and C. McCreight (NASA Center for AeroSpace Information, Hanover, MD, 2002), p. 173.
[8]D. Meledin *et al.*, IEEE Trans. Microwave Theory Tech. **52**, 2338 (2004).
[9]Herschel project on the web: http://www.esa.int/science/herschel or http://www.sron.rug.nl/hifiscience/
[10]E. M. Gershenzon, G. N. Gol'tsman, I. G. Gogidze, A. I. Eliantev, B. S. Karasik, and A. D. Semenov, Sverkhprovodimost' (KIAE) **3**, 2143 (1990) [Sov. Phys. Superconductivity **3**, 1582 (1990)].
[11]D. E. Prober, Appl. Phys. Lett. **62**, 2119 (1993).
[12]J. J. A. Baselmans, M. Hajenius, J. R. Gao, T. M. Klapwijk, P. A. J. de Korte, B. Voronov, and G. Gol'tsman, Appl. Phys. Lett. **84**, 1958 (2004).
[13]J. J. A. Baselmans, M. Hajenius, J. R. Gao, A. Baryshev, J. Kooi, T. M. Klapwijk, P. de Korte, B. Voronov, and G. Gol'tsman, IEEE Trans. Appl. Supercond. **15**, 484 (2005).
[14]S. Cherednichenko, P. Khosropanah, E. Kollberg, M. Kroug, and H. Merkel, Physica C **372–376**, 407 (2002).
[15]A. D. Semenov, H.-W. Hübers, J. Schubert, G. N. Gol'tsman, A. I. Elantiev, B. M. Voronov, and E. M. Gershenzon, J. Appl. Phys. **88**, 6758 (2000).
[16]G. Gol'tsman, Infrared Phys. Technol. **40**, 199 (1999).
[17]D. Wilms Floet, E. Miedema, T. M. Klapwijk, and J. R. Gao, Appl. Phys. Lett. **74**, 433 (1999).
[18]H. Merkel, P. Khosropanah, D. Wilms Floet, P. A. Yagoubov, and E. L. Kollberg, IEEE Trans. Microwave Theory Tech. **48**, 600 (2000).
[19]M. Hajenius, R. Barends, J. R. Gao, T. M. Klapwijk, J. J. A. Baselmans, A. Baryshev, B. Voronov, and G. Gol'tsman, IEEE Trans. Appl. Supercond. **15**, 495 (2005).
[20]R. Barends, M. Hajenius, J. R. Gao, and T. M. Klapwijk, Appl. Phys. Lett. **87**, 263506 (2005).
[21]K. Rohlfs, *Tools of Radio Astronomy* (Springer-Verlag, Berlin, 1986).
[22]R. Schieder and C. Kramer, Astron. Astrophys. **373**, 746 (2001).
[23]M. Hajenius, J. J. A. Baselmans, J. R. Gao, T. M. Klapwijk, P. A. J. de Korte, B. Voronov, and G. Gol'tsman, Supercond. Sci. Technol. **17**, 224 (2004).
[24]T. M. Klapwijk, R. Barends, J. R. Gao, M. Hajenius, and J. J. A. Baselmans, Proc. SPIE **5498**, 129 (2004).
[25]G. R. Boogaard, A. H. Verbruggen, W. Belzig, and T. M. Klapwijk, Phys. Rev. B **69**, 220503(R) (2004).
[26]Four terminal measurements on structures consisting of the identical layers have been performed to verify this claim.
[27]M. Hajenius, Z. Q. Yang, J. J. A. Baselmans, J. R. Gao, B. Voronov, and G. Gol'tsman, in *Proceedings of the 16th International Symposium on Space Terahertz Technology*, edited by M. Yngvarson, J. Stake, and H. Merkel (Chalmers University of Technology, Gothenburg, Sweden, 2005), p. 217.
[28]B. Jackson, J. Evers, and K. Wafelbakker, Document No. FPSS-00276, Issue: 1.1, Category: 3, (2002).
[29]W. F. M. Ganzevles, L. R. Swart, J. R. Gao, P. A. J. de Korte, and T. M. Klapwijk, Appl. Phys. Lett. **76**, 3304 (2000).
[30]P. Focardi, A. Neto, and W. R. McGrath, IEEE Trans. Microwave Theory Tech. **50**, 2374 (2002).
[31]M. J. M. van der Vorst, Ph.D. dissertation, Eindhoven University of Technology, (1999).
[32]W. Jellema, T. J. Finn, A. Baryshev, M. van der Vorst, S. Withington, J. A. Murphy, and W. Wild, in *Proceedings of the 16th International Symposium on Space Terahertz Technology*, edited by M. Yngvarson, J. Stake, and H. Merkel (Chalmers University of Technology, Gothenburg, Sweden, 2005), p. 398.
[33]P. F. Goldsmith, *Quasi-Optical Techniques at Millimeter and Submillimeter Wavelengths*, (Academic, New York, 1982), Chap. 7.
[34]Neal Erickson power meter model PM1B, Erickson Instruments, LLC 316 Pine St. Amherst, MA 01002.
[35]Thomas Keating Ltd., Station Mills, Billingshurst, UK, RH14 9SH (2005) (online available: www.terahertz.co.uk).
[36]A. R. Kerr, IEEE Trans. Microwave Theory Tech. **47–3**, 325 (1999).
[37]SRON/Kuo-Liang SN 2 with a bandwidth from 2.4 to 4.8 GHz, 25–26 dB of gain, and a 5 K noise temperature.
[38]S. Weinreb, MMIC LNA 2–14 GHz with 35–36 dB of gain and a noise temperature of 5 K.
[39]H. Ekström, B. S. Karasik, E. L. Kollberg, and K. S. Yngvesson, IEEE Trans. Microwave Theory Tech. **43**, 938 (1995).
[40]J. J. A. Baselmans *et al.*, Appl. Phys. Lett. **86**, 163503 (2005).
[41]J. Kawamura, C.-Y. E. Tong, R. Blundell, D. C. Papa, T. R. Hunter, F. Patt, G. Gol'tsman, and E. Gershenzon, IEEE Trans. Appl. Supercond. **11**, 952 (2001).
[42]QMC Instruments Ltd., Cardiff University, Cardiff, U.K.
[43]Z. Q. Yang, M. Hajenius, J. J. A. Baselmans, J. R. Gao, B. Voronov, and G. N. Gol'tsman, Semicond. Sci. Technol. **19**, L9 (2006).
[44]D. Loudkov, C.-Y. E. Tong, K. G. Megerian, and J. A. Stern, IEEE Trans. Appl. Supercond. **15**, 476 (2005).
[45]B. S. Karasik and A. I. Elantiev, Appl. Phys. Lett. **68**, 853 (1996).
[46]S. Cherednichenko *et al.*, 13th International Symposium on Space terahertz Technology, Harvard University, 2002 (unpublished), p. 85.
[47]J. W. Kooi, G. Chattopadhyay, M. Thielman, T. G. Phillips, and R. Schieder, Int. J. Infrared Millim. Waves **21**, 689 (2000).
[48]J. W. Kooi *et al.*, J. Appl. Phys. (in press).
[49]T. Berg, S. Cherednichenko, V. Drakinskiy, H. Merkel, E. Kollberg, and J. W. Kooi, *15th International Symposium on Space Terahertz Technology*, edited by G. Narayanan (University of Massachusetts, Amherst, MA, 2005), p. 25.